Magnetization behavior of ordered and high density Co nanowire arrays with varying aspect ratio

G. Kartopu, O. Yalçın, M. Es-Souni, and A. C. Başaran

Citation: Journal of Applied Physics **103**, 093915 (2008); doi: 10.1063/1.2917191
View online: http://dx.doi.org/10.1063/1.2917191
View Table of Contents: http://scitation.aip.org/content/aip/journal/jap/103/9?ver=pdfcov
Published by the AIP Publishing

Magnetization behavior of ordered and high density Co nanowire arrays with varying aspect ratio

G. Kartopu,[1,a)] O. Yalçın,[2] M. Es-Souni,[1] and A. C. Başaran[3]
[1]*Institute for Materials and Surface Technology, University of Applied Science Kiel, Grenzstrasse 3, 24149 Kiel, Germany*
[2]*Department of Physics, Bozok University, 66500 Yozgat, Turkey*
[3]*Department of Physics, Gebze Institute of Technology, 41400 Gebze, Kocaeli, Turkey*

(Received 19 December 2007; accepted 2 March 2008; published online 9 May 2008)

Densely packed and ordered cobalt nanowire (NW) arrays with aspect ratios (wire length/diameter) varying between 5 and 250 have been fabricated via electrodeposition into alumina templates. The wire length and diameter were controlled by monitoring the total deposited charge or by adjusting the template pore size, respectively. It is observed from room temperature magnetization curves that the magnetic properties of a given array is largely dependent on the aspect ratio and packing factor. It is shown that behavior of magnetic NW arrays are governed to a large extent by the magnetostatic interactions between NWs and that magnitude of the interaction field increases not only with NW diameter (or packing factor) but also with NW length. © *2008 American Institute of Physics*. [DOI: 10.1063/1.2917191]

I. INTRODUCTION

Currently, there is a rising interest in ferromagnetic nanowire (NW) arrays owing to their potential application in (perpendicular) data storage.[1] Self-assembly based *bottom-up* template synthesis techniques are highly appealing in this respect because they are relatively more simple and inexpensive compared to *top-down* lithography methods.[2] Particularly, electrodeposition into the pores of anodic alumina (AAO) templates can deliver size tunable and perpendicularly oriented NW arrays[3] with particle density exceeding $10^{11}/\mathrm{cm}^2$. While the diameter and density of particles can be tuned by the template parameters, their length and structure can be tailored via deposition parameters such as deposition time, applied bias, electrolyte content, and/or *p*H. Hitherto, nevertheless, magnetic studies involving template synthesized NWs are mainly focused on low-density arrays or even single NWs of transition metals,[4] with an aim to *isolate* and study the novel shape anisotropy effect and magnetization reversal mechanisms. Further, as for high density arrays, usually the magnetic behavior of very large aspect-ratio (wire length/diameter) wires is comparatively investigated between different metals (e.g., Ni versus Fe) and/or crystal structures [e.g., hexagonal-close-packed (hcp) Co versus face-centered-cubic (fcc) Co].[5–7] Therefore, more studies involving *densely packed* arrays are needed, for example, to understand the effect of geometrical factors, e.g., aspect ratio (wire length/diameter), packing density, etc., on array magnetic properties and to improve their potential in data storage applications.

Cobalt NW arrays form a particularly interesting system[8] as Co is a hard magnetic material with tailorable magnetic properties through variation of the structural parameters such as crystallinity, shape, and grain size. To exemplify, it was demonstrated in hcp Co NWs that depending on (crystal) texture, the shape and magnetocrystal anisotropies can either compete or add up to yield a partially controllable effective anisotropy.[9] Consequently, it has recently become a popular trend to try to control the orientation of hcp *c* axis (i.e., easy axis of the magnetocrystal anisotropy) and, hence, the effective anisotropy in Co NWs, for example, by applying a magnetic field during electrodeposition or by modifying the above-mentioned deposition parameters.[6,10–12]

In this study, we synthesized ordered and high density ($10^{10}/\mathrm{cm}^2$) Co NW arrays utilizing freestanding AAO templates and direct-current (dc) electrodeposition and investigated their magnetic properties as functions of NW aspect ratio (τ) and packing factor (or template porosity) by analyzing room temperature magnetization curves. (We note, however, that no special attention was paid to *engineer* the crystal structure/texture.) It is found that array magnetic properties are determined to a great extent by the magnetostatic interactions between array elements. We show that the interaction field can be effectively curbed by reducing not only the NW diameter (or packing factor) but also the NW length, thereby enhancing the potential of metal NW arrays in storage applications.

II. EXPERIMENTAL

Cobalt NWs were synthesized via dc electrodeposition into pore channels of ~60-μm-thick self-standing oxalic acid AAO templates prepared by the double-anodization method.[13] Briefly, anodization of high purity Al foils (99.999%) was carried out in 0.3*M* oxalic acid at 15 °C and 40 V. Following a long-term (first) anodization of 17 h, the sample was immersed in phosphoric acid:chromic acid mixture at 70 °C until the low quality oxide layer was completely dissolved. Second anodization was performed for 8 h, and subsequently, the nonoxidized portion of Al as well as the oxide barrier layer that was formed between Al and po-

a)Electronic mail: giray.kartopu@fh-kiel.de and gkartopu@hotmail.com. Present address: Bozok University, 66500 Yozgat, Turkey.

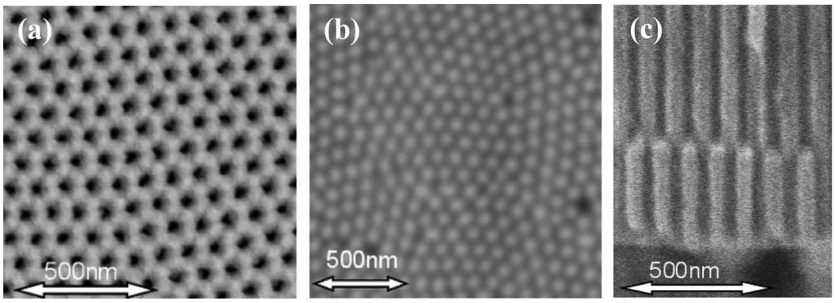

FIG. 1. Typical SEM images of an AAO template inside a domain (d=40 nm) (a) and Co NWs deposited inside AAO pore channels: topography (b) and cross-section (c).

rous alumina film was etched away to yield through-pore AAO membranes. For a set of samples, only a mild postanodization etching was applied in 5 wt. % H_3PO_4 solution (5 min) for rounding up the template pore channels, i.e., without substantially enlarging the pore diameter (d). Pore size in these membranes was determined to be d=40 nm. For a second set of samples, the pore size was controllably increased up to d=70 nm by changing the time of postanodization etching. In all samples, the pore center-to-center distance is ~105 nm.

As for the growth of Co NWs, first, a (thin) Au layer was sputter-deposited on one side of the membrane which was subsequently reinforced via electrodeposition with a thick (~1 μm) Cu film, as described elsewhere.[14,15] After sealing of the bare Cu surface (e.g., using nail polish) the sample was mounted in a conventional three-electrode cell with the *open-pore* side of AAO exposed to the electrolyte compartment. Prior to Co electrodeposition, the cell was filled with de-ionized water and ultrasonically agitated for 10 min in order to wet the pore channels and to ensure a homogenous metal deposition. Electrodeposition was carried out using an aqueous electrolyte containing 100 g/l $CoSO_4$ and 50 g/l H_3BO_3 at room temperature, under constant stirring, and at a bias of −1.1 V (versus Ag/AgCl). The wires grew in the usual bottom-up fashion starting from the Au electrode at the pore bottoms and the average wire length (L) was controlled by monitoring the total charge that passed during deposition. Several samples were prepared with wire lengths up to L =10 μm. (We note that with the employed deposition method filling efficiency became visibly poorer if $L<$ ~0.2 μm and, therefore, such samples were not selected for further analysis.) Several other samples were prepared using templates having different pore sizes where L was kept very high (>4 μm).

Microstructural characterization was performed using a Philips XL30 or Hitachi S-4800 field-emission scanning electron microscope (SEM). Cross-sectional SEM images of templates and NW arrays were simply collected by cleaving the specimens. Topographical images of the NW arrays were obtained by first grinding and then fine polishing AAO/Co composite samples containing sufficiently long NWs. Phase and crystallinity of NWs were checked by x-ray diffraction (XRD) θ-2θ scans utilizing a Seifert 3000 PTS four-circle-diffractometer (Cu $K\alpha$, λ=1.5418 Å). Hysteresis (M-H) loops were collected using a Quantum Design or ADE vibrating sample magnetometer at 300 K.

III. RESULTS AND DISCUSSION

Typical SEM micrographs of an ordered AAO template and Co NWs synthesized within AAO pores are shown in Fig. 1. The template exhibits hexagonally arranged pores with monodomain size of up to several μm^2. From topographical images, such as that in Fig. 1(b), it is determined that filling efficiency is better than 90%. In other words, only a small number of pores are blank (or *seem* empty but contain fairly short wires below the polished surface). Cross-sectional analyses of filled templates confirm the high degree of filling efficiency for all samples studied and show that wires conform to pore shape and are relatively uniform along their length [Fig. 1(c)]. Dispersion in wire length and wire diameter is determined to be around 15% and 10%, respectively.

The XRD profile of a specimen with L=10 μm and d =40 nm is shown in Fig. 2. Only a single peak is observable at 2θ=75.9°. It is not clear at present whether this peak corresponds to the (110) reflection of hcp structure or the (220) reflection of fcc structure of Co. According to available XRD library on (bulk) Co,[16] these two reflections are separated by only $2\theta<0.1°$. Although, it is known that at room temperature stable phase for bulk (or bulklike) Co is only hcp, in nanostructures or very thin films of Co, the fcc phase can also appear.[17] Therefore, also in line with the relevant literature involving low-d Co NWs,[5,6] it can be asserted that the single peak in Fig. 2 originates either from pure hcp or a combination of the hcp and fcc phases. Further, it can be inferred from the relatively small signal/noise in our spectra that the wires are not single crystals but rather consist of oriented polycrystals. Other weaker features in Fig. 2 are believed to originate from the partially crystalline alumina

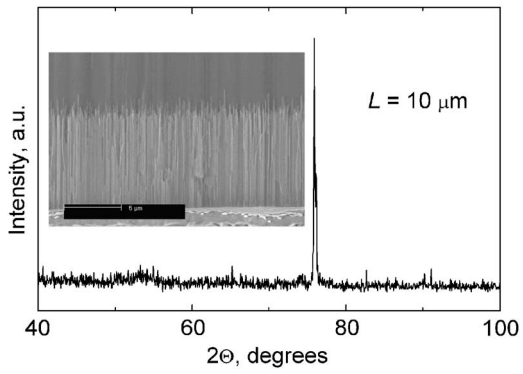

FIG. 2. XRD profile of an array with L=10 μm. Inset shows a cross-sectional SEM image of the XRD specimen (image bar: 5 μm).

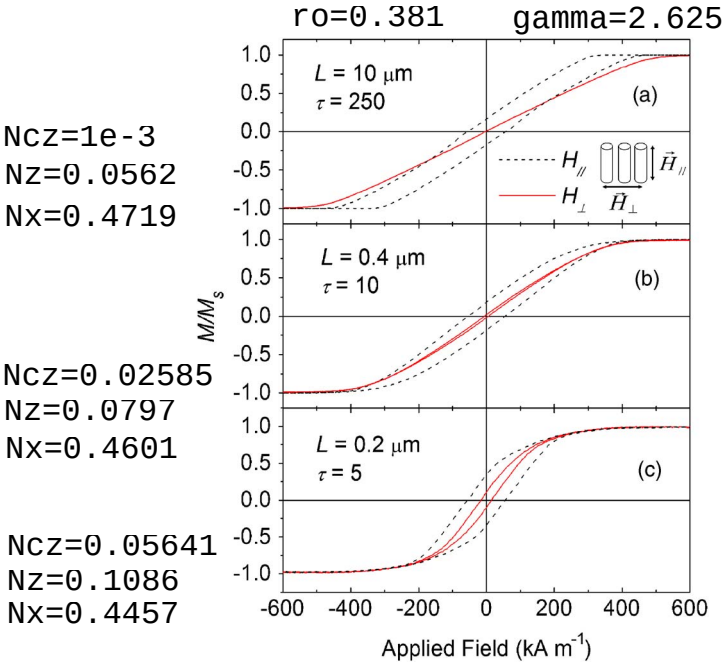

FIG. 3. (Color online) Normalized parallel and perpendicular hysteresis loops of Co NW arrays with $d=40$ nm and $L=10$ μm (a), 0.4 μm (b), and 0.2 μm (c).

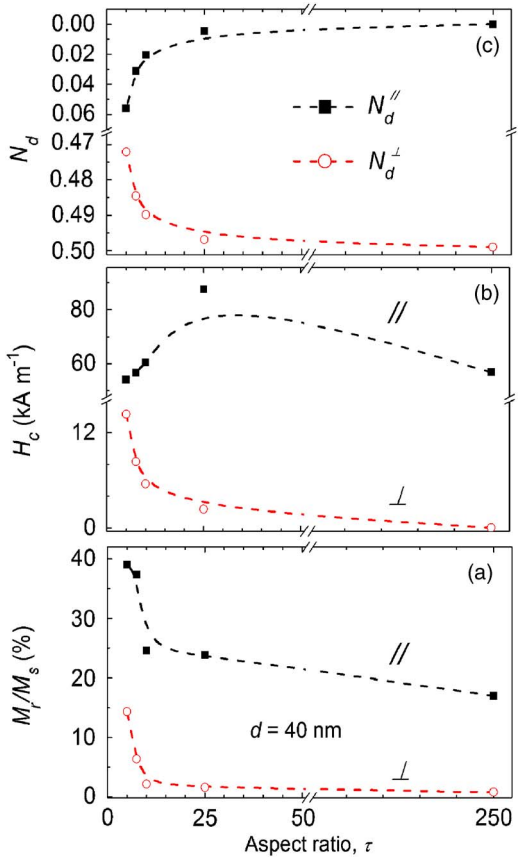

FIG. 4. (Color online) Squareness (M_r/M_s) (a) and coercive field (H_c) (b) for both parallel and perpendicular orientations as function of aspect ratio (or L); variation of demagnetization factors for a prolate spheroid particle (c).

template and/or the thick Cu film beneath the NW array. Further structural characterizations are needed in order to precisely determine the Co phase(s) and, e.g., the average size and texture of grains. It has been shown that transmission electron microscopy (TEM) combined with electron diffraction[18] (ED) or x-ray absorption spectroscopy[5] can serve well for detailed structural characterization of Co NWs. A combined TEM and ED study is underway.

Hysteresis loops of representative samples with $d=40$ nm and varying L are shown in Fig. 3. The sample with $L=10$ μm (aspect ratio $\tau=250$) exhibits a clear biaxial anisotropy. While hardly any magnetic hysteresis is observable when the applied field is in film plane (i.e., perpendicular to NW axis), a clear hysteresis can be seen for the out-of-plane orientation (i.e., field parallel to NW axis). Moreover, perpendicular saturation field ($\sim$560 kA m^{-1}) is close to that expected from shape anisotropy of an individual, infinitely long wire, that is $2\pi M_s=700$ kA m^{-1}, where M_s is the saturation magnetization of Co [note that at room temperature M_s (hcp Co)$=M_s$ (fcc Co)].[6] This observation is in line with previous reports involving long Co NWs.[19] Small reduction in saturation field can be attributed to the likely presence of other in-plane anisotropy fields (such as magnetocrystalline anisotropy), magnetostatic interactions between wires, and/or a reduction of M_s in nanoparticles. Contrary to squarelike (and wide) hysteresis loops of isolated (i.e., noninteracting) Co NWs (Ref. 10) the parallel hysteresis loops particularly for $L=10$ μm sample [Fig. 3(a)] are significantly sheared, hinting further on the presence of strong magnetostatic interactions between NWs. In the sample with $L=0.4$ μm ($\tau=10$), shearing of the parallel loop as well as saturation fields for both in-plane and out-of-plane geometries are slightly reduced while perpendicular loop starts to open up, i.e., its coercive field increases [Fig. 3(b)]. When the wire length is further reduced down to $L=0.2$ μm ($\tau=5$) almost an isotropic hysteric behavior is noted where perpendicular and parallel M-H curves become look alike as a result of the still-decreasing saturation fields and increasing out-of-plane coercivity [Fig. 3(c)]. Nevertheless, from the slightly wider coercive field and saturation field for the out-of-plane orientation, it can be suggested that the easy axis of magnetization in this sample remains parallel to the NW axis.

Evolution of coercivity (H_c) and loop squareness (M_r/M_s) (M_r is the remanent magnetization) with aspect ratio τ are plotted in Fig. 4. With decreasing τ (or L) while all $M_r/M_s^{\parallel}$, $M_r/M_s^{\perp}$, and $H_c^{\perp}$ increase, only $H_c^{\parallel}$ decreases (with exception of one data point). These changes monotonically occur first from $\tau=250$ to 25 and then rather abruptly from $\tau=25$ to 5 [Figs. 4(a) and 4(b)]. The smallest and largest values observed for $M_r/M_s^{\parallel}$ are 17% ($\tau=250$) and 39% ($\tau=5$), while 0.8% ($\tau=250$) and 14.3% ($\tau=5$) for $M_r/M_s^{\perp}$, 87.5 kA m^{-1} ($\tau=25$) and 54.1 kA m^{-1} ($\tau=5$) for $H_c^{\parallel}$, and 14.3 kA m^{-1} ($\tau=5$) and $\sim$0 kA m^{-1} ($\tau=250$) for $H_c^{\perp}$, respectively. Further, though it is unexpected (*vide infra*), most data points provided by the $\tau=250$ specimen seem to deviate from those of the sample with $\tau=25$. In high aspect ratio NWs shape anisotropy (or the self-demagnetization) energy density, given by $E_{SA}=M_s^2\Delta N/2$,[1,20] arises due to a strong difference between the demagnetization factors along and perpendicular to long axis (ΔN). We plot demagnetization factors for a cylinderlike object (prolate spheroid) as function of $\tau(=L/d)$ in Fig. 4(c). For $\tau > \sim 10$, $N_d^{\perp} \approx 0.5$ and $N_d^{\parallel} \approx 0$,

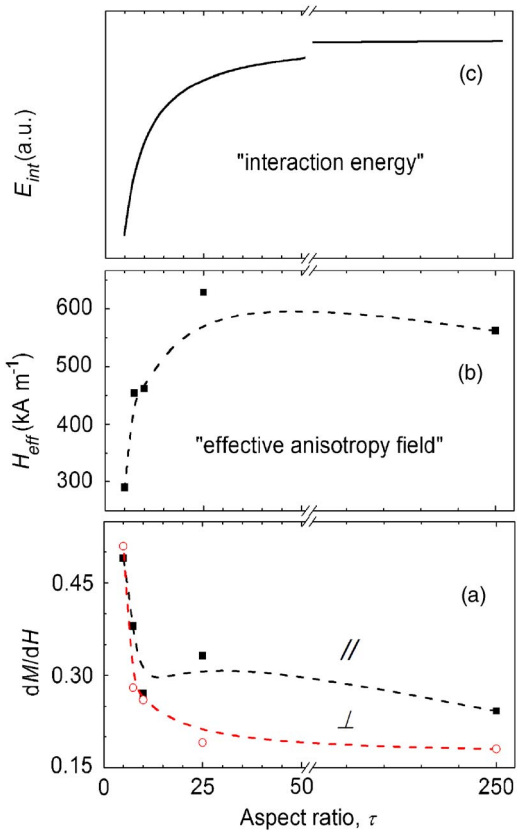

FIG. 5. (Color online) Slope (dM/dH) at $H=0$ A m^{-1} (a) and effective anisotropy field (H_{eff}) (b) as function of aspect ratio for Co NW arrays reported in Fig. 4. Variation of (calculated) magnetostatic interaction energy (E_{int}) with respect to aspect ratio for two parallel axially magnetized wires ($\rho \approx 0.4$) (c).

and for small τ, $N_d^{\perp}$ decreases while $N_d^{\parallel}$ increases with decreasing τ (and they unify around 0.33 at $\tau=1$).[1] In Fig. 4, there appears to be a good agreement between the evolutions of $N_d^{\perp}$ and $N_d^{\parallel}$ with τ and that experimentally observed for $H_c^{\perp}$ and $H_c^{\parallel}$, respectively [compare Figs. 4(b) and 4(c)]. Nevertheless, if results in Fig. 4 were to be explained only by the shape anisotropy effect, then would it be expected [from Fig. 4(c)] that specimens having $\tau=25$ and $\tau=250$ possessed the same magnetic parameters. Clearly, this is not the case. Further, the maximum relative change between the observed parallel and perpendicular coercivities with τ, namely, 50%, is clearly larger than that which occurs for calculated demagnetization factors (≈18%). Note also that the changes in both $M_r/M_s^{\parallel}$ and $M_r/M_s^{\perp}$ with τ [Fig. 4(a)] are greater than that expected from shape anisotropy.

For the same samples, the dependence of the effective anisotropy field H_{eff} (estimated from the intersection of parallel and perpendicular M-H curves) and the slope at zero applied field (dM/dH at $H \approx 0$) on τ are presented in Fig. 5. It can be seen in general that while both parallel and perpendicular slopes increase [Fig. 5(a)] the H_{eff} decreases [Fig. 5(b)] with decreasing τ, and that these gain speed at $\tau < \sim 25$.

These results can be better understood if one considers the presence and evolution of different anisotropies and magnetostatic interactions in NW arrays. In particular, for wires embedded inside nanotemplates, popularly known anisotropies, i.e., apart from the shape anisotropy, are the magnetocrystal and magnetoelastic anisotropies[1,20] which arise due to (crystal) texture and stress effects, respectively. Moreover, for nanoparticle arrays where distance between particles is comparable to particle size, magnetostatic interactions among them are (often) non-negligible[21] and contribute further to effective anisotropy. As for the present NW arrays, the wires are very uniform along their entire length, all of the sample parameters are kept constant but only τ is varied, and magnetic data were collected at the same temperature. It is thus reasonable to suggest that anisotropies other than shape anisotropy must remain effective to the same degree between arrays of different wire length (L). [However, the same cannot be said when arrays of different NW diameter (or packing factor) are compared, where particularly the magnetostatic (demagnetization) fields can be significantly variable (*vide infra*).]

Recently, within a Fourier space approach, Beleggia *et al.*[22] derived expressions to evaluate interaction energy (E_{int}) between a couple of magnetized nanoparticles of arbitrary shape. In Fig. 5(c), we plot E_{int} for two identical, parallel-lying and axially magnetized wires separated at an inverse distance of $\rho \approx 0.4$ calculated by the following expression [Eq. (58) in Ref. 22]:

$$E_{\text{int}} = \frac{\mu_0 |\boldsymbol{\mu}_1||\boldsymbol{\mu}_2|}{4\pi r^3} S_2(\rho, m), \tag{1}$$

where $\boldsymbol{\mu}_1 = \boldsymbol{\mu}_2$ are the magnetic moment of each wire (magnetization M times wire volume $V=\pi L d^2/4$), r and ρ ($=d/r$) are the direct and inverse (center-to-center) interwire distances, respectively, and $S_2(\rho, \tau)$ is a position and shape dependant correction factor which can be approximated for $\tau > 2$ to[22]

$$S_2(\rho,\tau) \approx \frac{1}{\tau^2}\left[\frac{2\tau^2\rho^2 - 1}{8(1+\tau^2\rho^2)^{5/2}} - \frac{2}{\rho^2\sqrt{1+\tau^2\rho^2}} + \frac{2}{\rho^2}{}_3F_2\left(\frac{1}{2},\frac{1}{2},\frac{2}{3};2,3;\rho^2\right)\right]. \tag{2}$$

Here, the ${}_3F_2\,[\cdots]$ term is a hypergeometric series and yields ~1.06 for $\rho^2=0.16$. From Fig. 5(c), it appears that for low τ, E_{int} is fairly small but it increases sharply with τ and saturates at $\tau \approx 50$. A fairly good agreement can be seen between the evolution of E_{int} [Fig. 5(c)] and that of magnetic data reported in Figs. 4 and 5, indicating the relevance and importance of interparticle interactions in determining magnetic properties of high-density ferromagnetic NW arrays.

To sum up, it appears that a cooperative *reduction* of self- and macroscopic-demagnetization fields is the cause of observed magnetic behaviors with decreasing wire length L (or τ). Observations made in a small number of previous reports also seem to support this assertion.[23,24] For example, Rivas *et al.*[24] prepared 200 and 400 nm diameter Co NW arrays (with interwire separations of $r \approx 480$ and 830 nm) in commercial polycarbonate membranes, and noted for both arrays a change in the direction of magnetization easy-axis from parallel- toward perpendicular-to-NW axis with increasing L. However, in order to evaluate the contribution of

(changing) magnetic interaction field to the observed behavior, they used a somewhat different and simpler formula $[H_{\text{int}} \approx 4.2(\text{MV}/r^3)]$ that is suited rather to describe the *dipolar* (interaction) fields in arrays of nanodots or very short cylindrical (wirelike) particles.[21] A recent theoretical study undertaken by Clime *et al.*[25] addressed the issue of magnetic interaction field experienced by a single wire within a fairly large (realistic) NW array. They compared their own results with experimental data of Ref. 23 and found a good agreement. This also brings confidence in our conclusion drawn above, that is the interaction field is inversely proportional to L or τ, in dense NW arrays. Here, we also like to note that a quantitative explanation of our results cannot be reached unless magnitudes of interaction and (relevant) anisotropy fields are determined using additional characterization methods. For this purpose, a detailed ferromagnetic resonance study is underway.

Finally, it follows from the above-presented results and discussions that it should be possible to tune the magnetic properties of NW arrays also by altering the inverse distance ρ or, in other words, the packing factor (f). Indeed, for example, Nielsch *et al.*[26] prepared high aspect ratio Ni NW arrays in oxalic acid AAO templates with different porosities and observed that out-of-plane M-H curves become more square showing larger coercivity ($H_c^{\parallel}$) and squareness ($M_r/M_s^{\parallel}$) with decreasing ρ (where NW diameter d was changed from 50 to 40 to 30 nm). We attested these findings in Co NW arrays. Several Co NWs samples (having $\tau > 50$) were obtained under identical deposition conditions using templates with adjusted pore size (or porosity). Figure 6(a) shows some example M-H curves where one can clearly see a systematic change of magnetization easy axis from out-of-plane ($d=40$ nm and $\rho \approx 0.4$) to in-plane orientation ($d=70$ nm and $\rho \approx 0.7$). With increasing ρ, in-plane saturation field decreases (with perpendicular loop becoming more square) and out-of-plane saturation field dramatically rises (with parallel loop becoming more sheared). As a result, H_{eff} increases from around 560 to 1030 kA m^{-1} with increasing ρ (or d) [Fig. 6(b)]. Even though the sample with the thickest wires ($d=70$ nm) behaves similar to bulklike ferromagnetic thin films by exhibiting strong in-plane easy axis, the out-of-plane (in-plane) coercivity still remains large (small), viz., $H_c^{\parallel}=26.6$ kA m^{-1} ($H_c^{\perp}=4.6$ kA m^{-1}). This can be attributed to the wirelike nature of the studied films. Thus, apparent differences between respective hysteresis loops in Fig. 6 should primarily be attributed to the evolution of magnetic interactions with ρ. Dramatic increase of the interaction field also remarkably lowers the out-of-plane coercivity ($H_c^{\parallel}$).

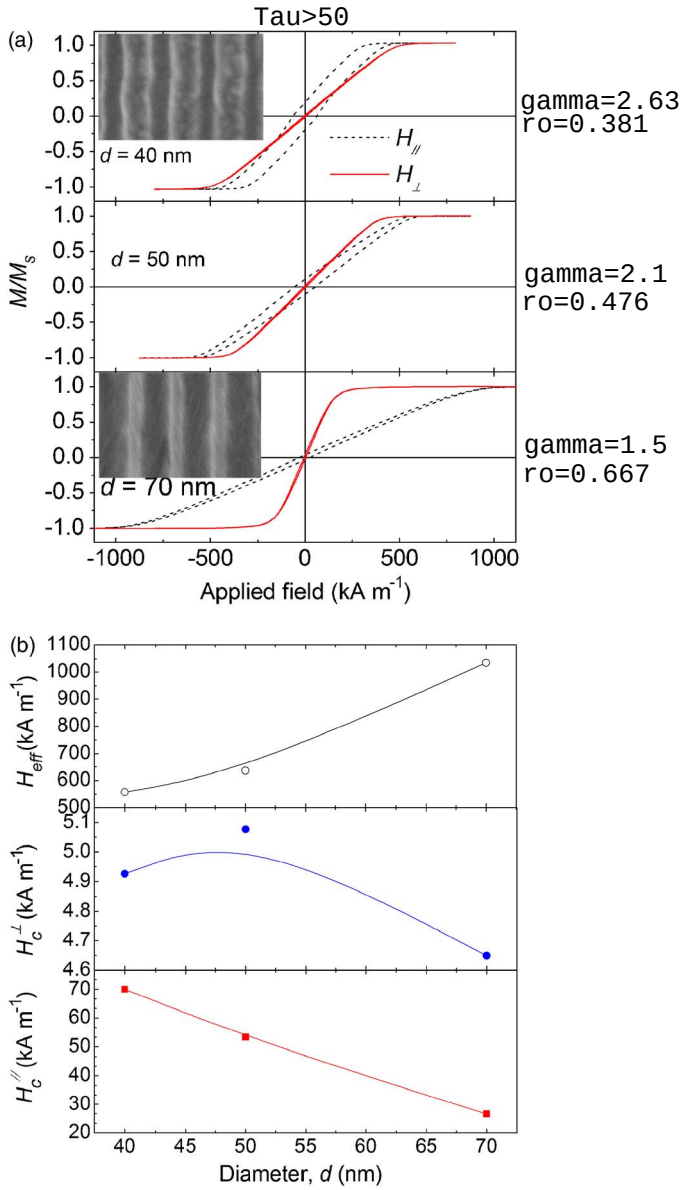

FIG. 6. (Color online) Normalized M-H curves of high aspect ratio ($\tau > 50$) Co NW arrays with $d=40-70$ nm ($\rho \approx 0.4-0.7$) (a), and extracted magnetic parameters (b). Insets in (a) show cross-sectional SEM images of the used templates with 40 and 70 nm pores (image sizes are identical at 360×230 nm^2, dark lines correspond to pores, and columns correspond to pore walls).

IV. CONCLUSION

Densely packed Co NW arrays of varying length L and diameter d were obtained via dc electrodeposition inside the pores of an ordered oxalic acid AAO template with 105 nm center-to-center pore distance (r). Dependence of magnetic properties on L and d, i.e., aspect ratio τ and packing factor f, was investigated (in the range $\tau=5-250$) using a vibrating sample magnetometer at room temperature. It was observed that, in most cases, the magnetization easy axis lie parallel to NW axis and that magnetic parameters, including coercivity, squareness, slope at zero field, and effective anisotropy field are highly correlated (and hence can be effectively controlled) with τ and f. Magnetostatic interactions between NWs as well as shape anisotropy effects are shown to determine the magnetic properties of a given array. Specifically, the interaction field increases not only with d but also with L. Our results are in good agreement with recent theories and previous experimental observations made by others.

ACKNOWLEDGMENTS

This work was funded by EU Interreg III NANODE project. We are thankful to Professor H.-G. Rubahn and Mr.

M. Madsen, Southern Denmark University, for FE-SEM analysis, and to Dr. J. Krause, at FH-Kiel, for useful discussions.

[1]L. Sun, Y. Hao, C.-L. Chien, and P. C. Searson, IBM J. Res. Dev. **49**, 79 (2005).
[2]T. M. Whitney, J. S. Jiang, P. C. Searson, and C. L. Chien, Science **261**, 1316 (1993); T. Thurn-Albrecht, J. Schotter, G. A. Kästle, N. Emley, T. Shibauchi, L. Krusin-Elbaum, K. Guarini, C. T. Black, M. T. Tuominen, and T. P. Russell, *ibid.* **290**, 2126 (2000).
[3]G. Kartopu, S. Habouti, and M. Es-Souni, Mater. Chem. Phys. **107**, 226 (2008).
[4]R. Ferre, K. Ounadjela, J. M. George, L. Piraux, and S. Dubois, Phys. Rev. B **56**, 14066 (1997), and references therein.
[5]R. E. Benfield, D. Grandjean, J. C. Dore, Z. Wu, M. Kröll, T. Sawitowski, and G. Schmid, Eur. Phys. J. D **16**, 399 (2001); M. Kröll, W. J. Blau, D. Grandjean, R. E. Benfield, F. Luis, P. M. Paulus, and L. J. de Jongh, J. Magn. Magn. Mater. **249**, 241 (2002).
[6]F. Li, T. Wang, L. Ren, and J. Sun, J. Phys.: Condens. Matter **16**, 8053 (2004), and references therein.
[7]J. H. Min, J. U. Cho, Y. K. Kim, J.-H. Wu, Y.-D. Ko, and J.-S. Chung, J. Appl. Phys. **99**, 08Q510 (2006).
[8]O. Yalçın, F. Yıldız, M. Özdemir, B. Aktaş, Y. Köseoğlu, M. Bal, and M. T. Touminen, J. Magn. Magn. Mater. **272–276**, 1684 (2004).
[9]S. Ge, C. Li, X. Ma, W. Li, L. Xi, and C. X. Li, J. Appl. Phys. **90**, 509 (2001), and references therein.
[10]M. Darques, A. Encinas, L. Vila, and L. Piraux, J. Phys. D **37**, 1411 (2004).
[11]J. U. Cho, J. H. Min, S. P. Ko, J. Y. Soh, Y. K. Kim, J.-H. Wu, and S. H. Choi, J. Appl. Phys. **99**, 08C909 (2006).
[12]V. R. Caffarena, A. P. Guimarães, W. S. D. Folly, E. M. Silva, and J. L. Capitaneo, Mater. Chem. Phys. **107**, 297 (2008).
[13]H. Masuda and K. Fukuda, Science **268**, 1466 (1995).
[14]G. Kartopu, M. Es-Souni, A. V. Sapelkin, and D. Dunstan, Phys. Status Solidi A **203**, R82 (2006).
[15]G. Kartopu, M. Es-Souni, A.V. Sapelkin, and D. Dunstan, J. Nanosci. Nanotechnol. **8**, 931 (2008).
[16]International Powder Diffraction Files JCPDS Card No. 05-0727(unpublished); International Powder Diffraction Files JCPDS Card No. 15-0806 (unpublished).
[17]D. Shi, B. Aktaş, L. Pust, and F. Mikailov *Nanostructured Magnetic Materials and Their Applications* (Springer-Verlag, Berlin, 2002); P. Bruno, G. Bayreuther, P. Beauvillain, C. Chappert, G. Lugert, D. Renard, J. P. Renard, and J. Seiden, J. Magn. Magn. Mater. **93**, 605 (1991).
[18]M. Darques, L. Piraux, A. Encinas, P. Bayle-Guillemaud, A. Popa, and U. Ebels, Appl. Phys. Lett. **86**, 072508 (2005).
[19]H. Zeng, M. Zeng, R. Skomski, D. J. Sellmyer, Y. Liu, L. Menon, and S. Bandyopadhyay, J. Appl. Phys. **87**, 4718 (2000); H. Zeng, R. Skomski, L. Menon, Y. Liu, S. Bandyopadhyay, and D. J. Sellmyer, Phys. Rev. B **65**, 134426 (2002).
[20]A. Kumar, S. Fähler, H. Schlörb, K. Leistner, and L. Schultz, Phys. Rev. B **73**, 064421 (2006).
[21]M. Grimsditch, Y. Jaccard, and K. Ivan Schuller, Phys. Rev. B **58**, 11539 (1998), and reference therein.
[22]M. Beleggia, S. Tandon, Y. Zhu, and M. De Graef, J. Magn. Magn. Mater. **278**, 270 (2004).
[23]G. J. Strijkers, J. H. J. Dalderop, M. A. A. Broeksteeg, H. J. M. Swagten, and W. J. M. de Jonge, J. Appl. Phys. **86**, 5141 (1999).
[24]J. Rivas, A. Kazadi Mukenga Bantu, G. Zaragoza, M. C. Blanco, and M. A. López-Quintela, J. Magn. Magn. Mater. **249**, 220 (2002).
[25]L. Clime, P. Ciureanu, and A. Yelon, J. Magn. Magn. Mater. **297**, 60 (2006).
[26]K. Nielsch, R. B. Wehrsohn, J. Bartel, J. Kirschner, U. Gösele, S. F. Fischer, and H. Kronmüller, Appl. Phys. Lett. **79**, 1360 (2001).